

Kinematic selection criteria in a new resonance searches: Application to pentaquark states

Boris Levchenko

Skobeltsyn Institute of Nuclear Physics, Moscow State University

Abstract

In this note I recall some features of two-body decay kinematics which can be effectively applied, in particular, in experimental searches for pentaquark states.

1 Introduction

In experimental searches for resonances, tracks of secondary particles are combined to form resonance candidates. In high energy reactions with multiparticle final states, this method of resonance reconstruction may cause a huge combinatorial background. Any additional physical information about the resonance and its decays (life-time, the mass of secondary particles etc.) helps considerably to reduce the background. For instance, the presence in an event a well separated secondary vertex allows us to reconstruct Λ , K_s and mesons from the D -meson family with a very low background. One such example is in Ref. [1]. Moreover, if masses of decay products are known and significantly differ from each other, this information also has to be used to reduce the background. This note is a discussion of these issues.

Below only two-body decays are considered and for each final state particle a set of equations describing boundaries of the physical region is given. Features of each physical region, through implementation in selection criteria, can be used in the background suppression.

2 Two particle decay

Let us consider a two-particle decay, $R \rightarrow \mathbf{a} + \mathbf{b}$, of a resonance R with a mass M_R and a momentum \vec{P}_R in the laboratory frame. Masses of the decay products are denoted as $m_{\mathbf{a}}$ and $m_{\mathbf{b}}$. At the rest frame of R the particles \mathbf{a} and \mathbf{b} are flying in opposite directions with the momentum [2]

$$P^* = \frac{1}{2M_R} [(M_R^2 - m_{\mathbf{a}}^2 - m_{\mathbf{b}}^2)^2 - 4m_{\mathbf{a}}^2 m_{\mathbf{b}}^2]^{1/2} \quad (1)$$

In the laboratory frame, the absolute momenta $p_{\mathbf{a}}$ and $p_{\mathbf{b}}$ of the particles \mathbf{a} and \mathbf{b} depend on the relative orientation of the rest frame vectors $\vec{p}_{\mathbf{a}}^*$ and $\vec{p}_{\mathbf{b}}^*$ with respect to the boost vector. We shall consider only Lorentz boosts along the momentum \vec{P}_R and denote by $\theta_{\mathbf{a}}^*$ the polar angle between $\vec{p}_{\mathbf{a}}^*$ and the direction given by \vec{P}_R . In that case, $\theta_{\mathbf{b}}^* = \pi - \theta_{\mathbf{a}}^*$.

The energy and momentum components in both frames are related via [2]

$$E_{\mathbf{a}(b)} = \gamma E_{\mathbf{a}(b)}^* - \vec{\eta} \cdot \vec{p}_{\mathbf{a}(b)}^* \quad (2)$$

$$\vec{p}_{\mathbf{a}(\mathbf{b})} = \vec{p}_{\mathbf{a}(\mathbf{b})}^* + \vec{\eta} \left[\frac{\vec{\eta} \cdot \vec{p}_{\mathbf{a}(\mathbf{b})}^*}{\gamma + 1} - E_{\mathbf{a}(\mathbf{b})}^* \right] \quad (3)$$

For a boost along \vec{P}_R , the boost parameters are

$$\gamma = \frac{E_R}{M_R}, \quad \vec{\eta} = -\frac{\vec{P}_R}{M_R} \quad (4)$$

and therefore

$$p_{\mathbf{a}(\mathbf{b})} = \frac{1}{M_R} \sqrt{(E_R E_{\mathbf{a}(\mathbf{b})}^* + P_R P^* \cos \theta_{\mathbf{a}(\mathbf{b})}^*)^2 - m_{\mathbf{a}(\mathbf{b})}^2 M_R^2} \quad (5)$$

If in an experiment there is no possibility to determine a particle type corresponding to a given charged track, then only information about the particle momentum, Eq.(5), is used. In the opposite case, when the particle type can be identified, for instance, by ionization, time of flight etc., one may incorporate this information and in addition use Eq. (2). Below, these cases are considered separately.

2.1 Particles without identification

The boundaries of the physical regions of the particle \mathbf{a} on the $(P_R, p_{\mathbf{a}})$ plane are easy to obtain with the use of the equation (5). For a given P_R , $p_{\mathbf{a}}$ reaches the upper limit at $\theta_{\mathbf{a}}^* = 0$

$$p_{\mathbf{a}}^+ = \frac{1}{M_R} (P_R E_{\mathbf{a}}^* + E_R P^*) \quad (6)$$

when the lower limit at $\theta_{\mathbf{a}}^* = \pi$

$$p_{\mathbf{a}}^- = \frac{1}{M_R} |P_R E_{\mathbf{a}}^* - E_R P^*| \quad (7)$$

The equations similar to (6)-(7) are valid for the particle \mathbf{b} too. At the resonance rest frame (7) demonstrates an interesting feature of the momentum of the particle flying backward. With increasing P_R , the momentum $p_{\mathbf{a}}$ ($p_{\mathbf{b}}$) first decreases, at $P_R = M_R P^* / m_{\mathbf{a}(\mathbf{b})}$ it reaches the zero value and only at larger P_R starts to increase. When plotted on the momentum $(P_R, p_{\mathbf{a}})$ plane, Eqs.(6)-(7) select a band-like physical region (m -band). For secondary particles with equal masses, $m_{\mathbf{a}} = m_{\mathbf{b}}$, these m -bands are fully overlapping. However, if for instance, $m_{\mathbf{a}} > m_{\mathbf{b}}$, the m -bands overlap only partially or even separate out at

$$P_R \geq P_R^{(s)} = \frac{2M_R P^*}{\sqrt{(E_{\mathbf{a}}^* - E_{\mathbf{b}}^*)^2 - 4(P^*)^2}} \quad (8)$$

The last equation follows from the condition $p_{\mathbf{a}}^- \geq p_{\mathbf{b}}^+$. In Eq (8) the expression under the square root is positive only if

$$P^* < \frac{m_{\mathbf{a}}^2 - m_{\mathbf{b}}^2}{\sqrt{8(m_{\mathbf{a}}^2 + m_{\mathbf{b}}^2)}} \quad (9)$$

Thus, for $m_{\mathbf{a}} \gg m_{\mathbf{b}}$ the physical regions of the particle \mathbf{a} and \mathbf{b} do not overlap if

$$m_{\mathbf{a}} \geq \sqrt{8} P^* \quad (10)$$

and $P_R > P_R^{(s)}$.

We shall now consider a few particular applications of equations (6)-(10). According to the PDG [3] only resonances with mass close to the threshold value $m_{\mathbf{a}} + m_{\mathbf{b}}$ satisfy the condition (10). Some of them are listed in Table 1, where P^* and $P_R^{(s)}$ values were calculated with use of (1) and (8), respectively.

Table 1

$R \rightarrow \mathbf{a} + \mathbf{b}$	M_R , GeV	$m_{\mathbf{a}}$, GeV	$\sqrt{8}P^*$, GeV	$P_R^{(s)}$, GeV
$\Lambda \rightarrow p + \pi^-$	1.115	0.938	0.284	0.301
$\Delta \rightarrow N + \pi$	1.232	0.939	0.643	1.052
$\Sigma \rightarrow N + \pi$	1.193	0.939	0.528	0.714
$\Sigma \rightarrow \Lambda + \pi$	1.385	1.115	0.596	0.752
$\Sigma \rightarrow N + K$	1.480	0.939	0.494	2.066
$D^0 \rightarrow a_1(1260)^+ + K^-$	1.865	1.230	0.924	6.457
$D^{*\pm} \rightarrow D^0 + \pi^\pm$	2.010	1.865	0.107	0.088
$D_{s1}^+ \rightarrow D^*(2010)^+ + K^0$	2.535	2.010	0.424	0.519
...

Figs. 1a , 1b and 1c shows m -bands of decay products for some resonances listed in Table 1. For all of them always

$$p_{\mathbf{a}} > p_{\mathbf{b}} \quad (11)$$

at $P_R > P_R^{(s)}$, and $m_{\mathbf{a}}$ significantly larger than $m_{\mathbf{b}}$. We will refer to the momentum condition (11) as a m -selector. Thus, for resonances of the type in Table 1, fulfillment of the condition (11) allows an assignment to the particle \mathbf{a} of the mass $m_{\mathbf{a}}$, i.e. we identify the particle \mathbf{a} . The m -selector (11) is a powerful tool for background suppression.

In the two-body decay modes one meet with a higher incidence the situation shown in Fig. 1d. For these decays the conditions (9)-(10) are not fulfilled and at any P_R the phase space bands remain overlapping. Nevertheless, if $m_{\mathbf{a}} > m_{\mathbf{b}}$, one can demand fulfillment of (11) for the particle \mathbf{a} in order to assign it the mass $m_{\mathbf{a}}$. In course of the resonance search the condition (11) rejects not only a significant part of the background, but also some fraction of the signal combinations. To estimate the efficiency of the m -selector we proceed in the following way.

On $(P_R, p_{\mathbf{a}})$ plane the condition (11) is valid up to the line defined by the equation

$$p_{\mathbf{a}}(\cos\theta_{\mathbf{a}}^*, P_R) = p_{\mathbf{b}}(\cos\theta_{\mathbf{b}}^*, P_R) \quad (12)$$

For $K^* \rightarrow K\pi$ decays the last equality is shown in Fig. 1d by the dashed line. The true K^* is a combination of a kaon from the region above the line (12) with a pion below it, and vice versa. From (12) and (5) we find the variation of $\theta_{\mathbf{a}}^* = \pi - \theta_{\mathbf{b}}^*$ along the line (12)

$$\cos\hat{\theta}_{\mathbf{a}}^* = -\frac{P_R}{E_R} \cdot \frac{(E_{\mathbf{a}}^* - E_{\mathbf{b}}^*)}{2P^*} \quad (13)$$

At the rest frame of R , (11) is equivalent to the exclusion of the region $\theta_{\mathbf{a}}^* > \hat{\theta}_{\mathbf{a}}^*$. For unpolarized particles the distribution of $\cos\theta_{\mathbf{a}}^*$ is uniform and we define the efficiency of the m -selector (11) as

$$E_{ff} = \frac{1 - \cos\hat{\theta}_{\mathbf{a}}^*}{2} \cdot 100\% \quad (14)$$

With the definition (14) we get $E_{ff} = 100\%$, when the conditions (9)-(10) are fulfilled, and $E_{ff} = 50\%$ for decays with $m_{\mathbf{a}} = m_{\mathbf{b}}$ ¹. As another example, in Fig. 4 by the dashed line is shown the evolution of E_{ff} with P_R in $K^* \rightarrow K\pi$ decays. E_{ff} grows because with the increase of P_R the overlap of m -bands decreases.

¹For real data $E_{ff} < 50\%$, see discussion in Sec.3

In the limit large P_R , the expression for the efficiency can be simplified:

$$E_{ff} = \frac{1}{2} \left(1 + \frac{m_{\mathbf{a}}^2 - m_{\mathbf{b}}^2}{\sqrt{[M_R^2 - (m_{\mathbf{a}} - m_{\mathbf{b}})^2] [M_R^2 - (m_{\mathbf{a}} + m_{\mathbf{b}})^2]}} \right) \cdot 100\% \quad (15)$$

$$\simeq \frac{1}{2} \cdot \frac{M_R^2}{M_R^2 - m_{\mathbf{a}}^2} \cdot 100\% \quad (16)$$

The last equation is a good approximation only if $m_{\mathbf{a}} \gg m_{\mathbf{b}}$. Equations (15)-(16) confirms the result we have already seen in Fig. 4a, where E_{ff} is independent of P_R at large P_R . On the other hand, for fixed values of $m_{\mathbf{a}}$ and $m_{\mathbf{b}}$, E_{ff} decreases with increasing M_R , the mass of the resonance candidate. Thus, the higher the invariant mass of a two-particle combination, the more strongly (11) suppresses that part of the mass spectrum.

2.2 Identified particles

Accounting for the particle masses² transforms Eqs (6)-(7) into

$$E_{\mathbf{a}}^+ = \frac{1}{M_R} (E_R E_{\mathbf{a}}^* + P_R P^*) \quad (17)$$

$$E_{\mathbf{a}}^- = \frac{1}{M_R} (E_R E_{\mathbf{a}}^* - P_R P^*) \quad (18)$$

and at low P_R leads to a 'repulsion' between the phase space E -bands on the energy ($P_R, E_{\mathbf{a}}$) plane (Fig. 2). For all resonances with $m_{\mathbf{a}} \gg m_{\mathbf{b}}$ (see Table 1)

$$E_{\mathbf{a}} > E_{\mathbf{b}} \quad (19)$$

independently of P_R . This is not always true for the background combinations. Therefore, if applied, the condition (19) suppresses the background even more strongly than (11). We will refer to the energy condition (19) as a E -selector.

As in the previous section, if the masses of the secondary particles do not differ significantly, at P_R greater than

$$\hat{P}_R = \frac{M_R(E_{\mathbf{a}}^* - E_{\mathbf{b}}^*)}{\sqrt{4(P^*)^2 - (E_{\mathbf{a}}^* - E_{\mathbf{b}}^*)^2}} \quad (20)$$

the E -bands start overlapping in the way shown in Fig 2d. The loss of signal combinations by demanding (19) for resonance candidates we estimate again with Eq. (14). In the case under consideration, $\cos\hat{\theta}_{\mathbf{a}}^*$ is a solution of the equation

$$E_{\mathbf{a}}(\cos\theta_{\mathbf{a}}^*, P_R) = E_{\mathbf{b}}(\cos\theta_{\mathbf{b}}^*, P_R) \quad (21)$$

Thus

$$\cos\hat{\theta}_{\mathbf{a}}^* = -\frac{E_R}{P_R} \cdot \frac{(E_{\mathbf{a}}^* - E_{\mathbf{b}}^*)}{2P^*} \quad (22)$$

In the limit large P_R , with (22) we again recover Eqs. (15)-(16). The evolution of E_{ff} in $K^* \rightarrow K\pi$ decays is shown in Fig. 4a by the full line. $E_{ff} = 100\%$ at $P_R < \hat{P}_R$ and drops down up to the value (15), $E_{ff} \simeq 71\%$, with increase of P_R .

²The author is grateful to S.Chekanov for a discussion of that subject.

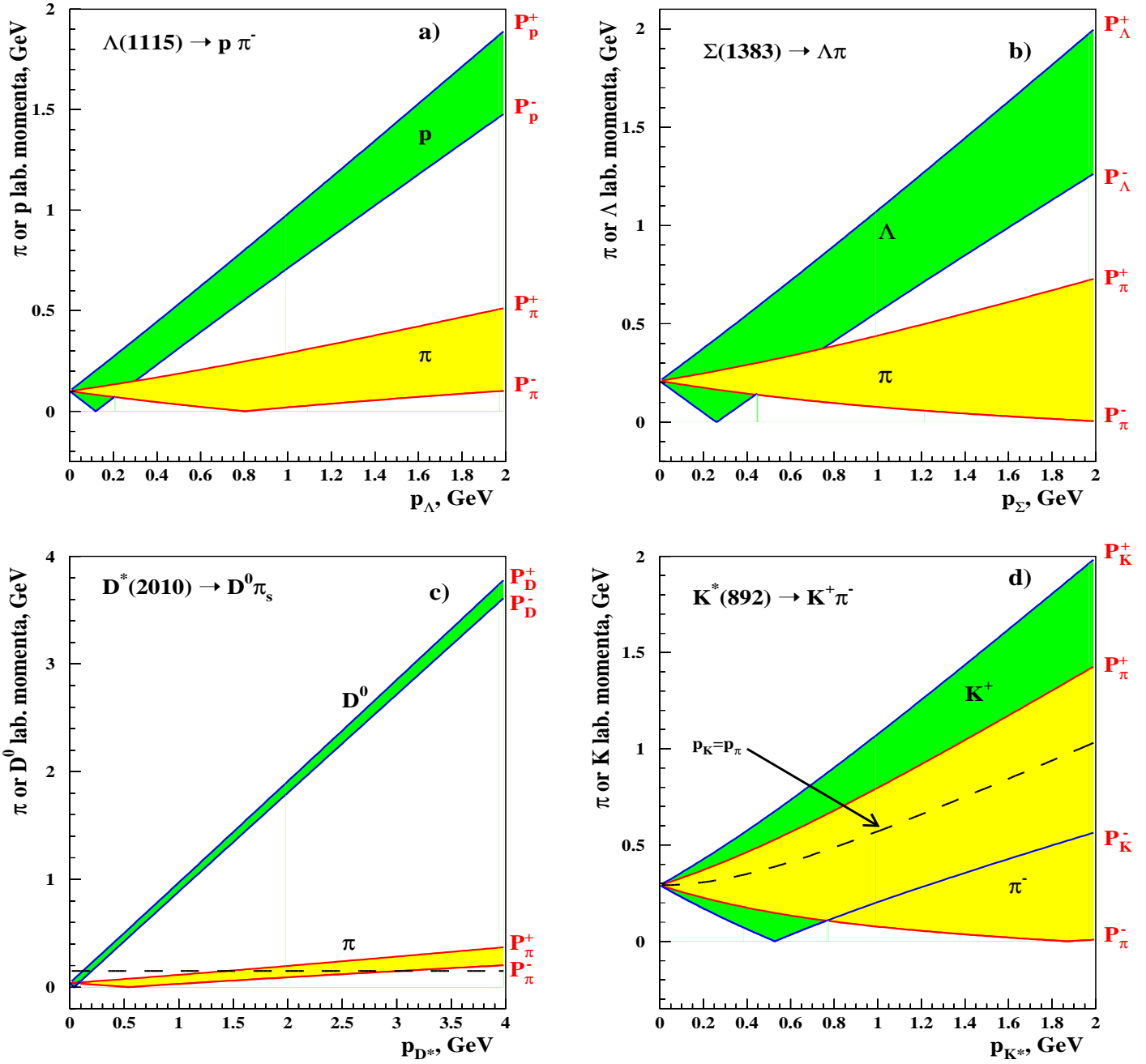


Figure 1: Phase space m -bands of the particle **a** and **b** in the decays $R \rightarrow \mathbf{a} + \mathbf{b}$ as a function of the resonance momentum P_R . The dashed line on (c) corresponds to the momentum cut $p_\pi = 0.15$ GeV (See Section 3). The dashed line on (d) is correspond to Eq.(12).

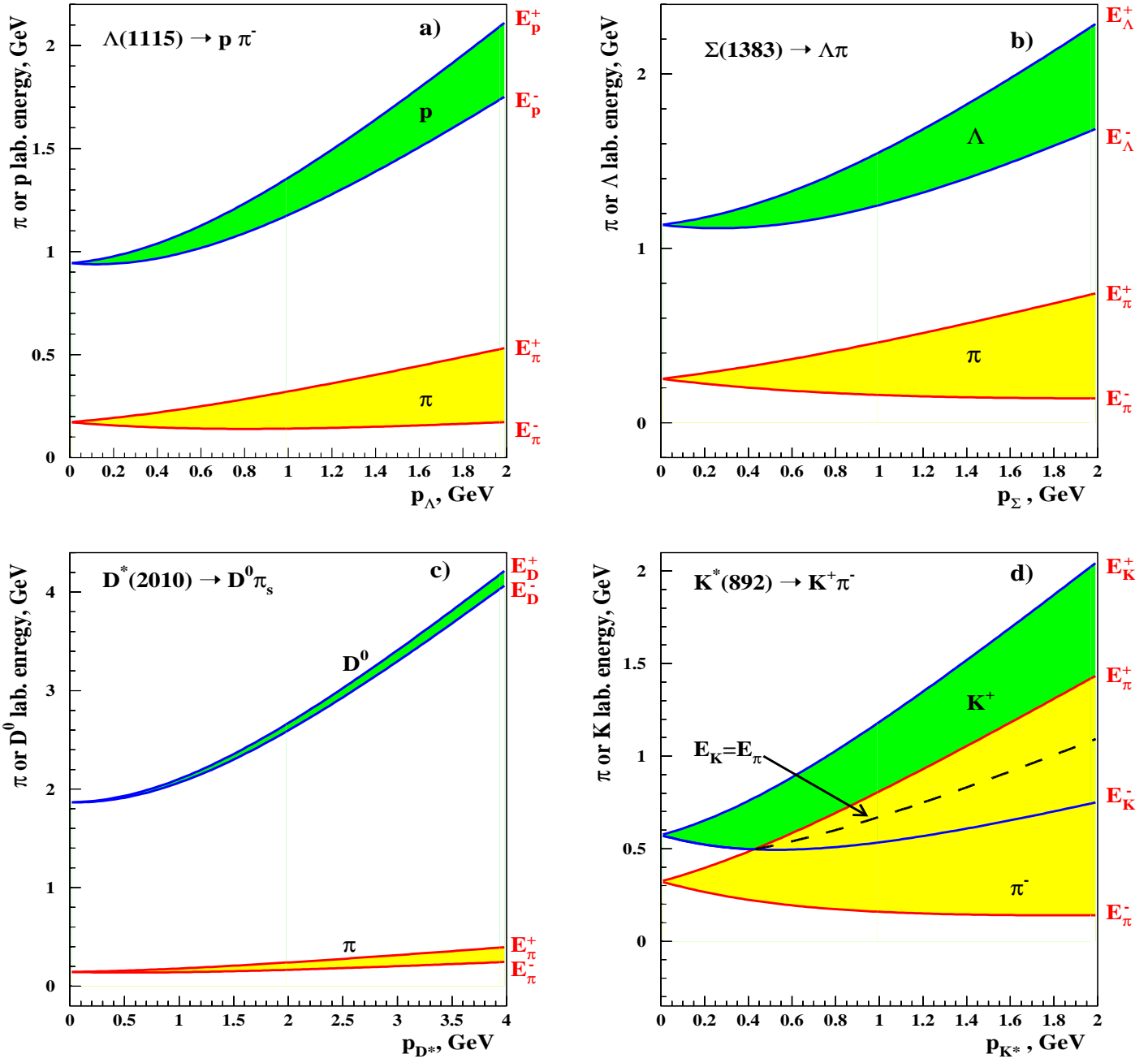


Figure 2: Phase space E-bands in $R \rightarrow a + b$ decays as a function of the resonance momentum P_R . The dashed line on (d) corresponds to Eq.(21).

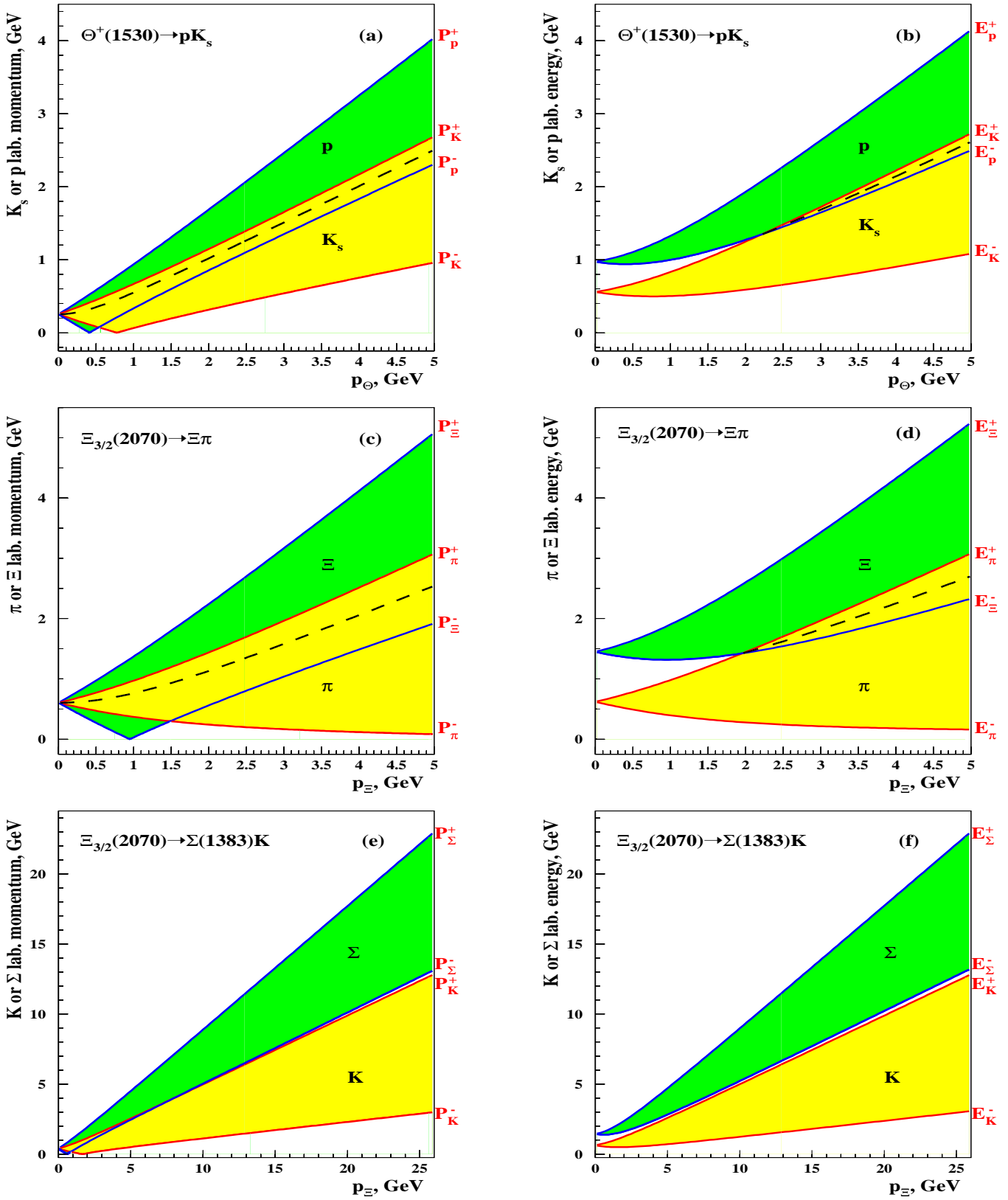


Figure 3:Phase space m -bands ((a), (c), (e)) and E -bands ((b), (d), (f)) in decays of the pentaquark states $\Theta(1530)$ and $\Xi_{3/2}(2070)$. The dashed lines correspond to Eqs.(12) and (21).

3 Remark about D^* reconstruction

Charged particles are tracked in a tracking detector (TD). The resolution of the transverse momentum of a track traversing the TD is parametrized by $\sigma(p_T)/p_T = Ap_T \oplus B \oplus C/p_T$, with p_T being the track transverse momentum (in GeV). The coefficients A , B and C characterize the resolution of the TD. Usually, to increase the momentum resolution, only tracks with $p_T > 0.12 - 0.15$ GeV are selected. That cut, as shown in Fig. 1c, make impossible the reconstruction of D^* mesons with momenta lower than 1.8-2.0 GeV. The m -band of π mesons is very narrow and grows rather slowly with P_R . Tracks with momenta greater than $p_\pi^+(P_{D^*})$ belong to the background. This property can be used to suppress the background contribution to the distribution of the mass difference, $\Delta M = M(K\pi\pi_s) - M(K\pi)$, by applying to the momentum of the soft pion (π_s) the following cut

$$p_{\pi_s} < p_0 + p_\pi^+(P_{D^*}) \quad (23)$$

where $p_0=0.0-0.3$ GeV is a some shift from the pion m -band. In the decay $D^* \rightarrow D^0\pi$, the rest frame momentum is small, $P^*=0.038$ GeV, and the D^* momentum can be estimated with (6) by means of the reconstructed D^0 momentum,

$$P_{D^*} = \frac{M_{D^*}}{M_{D^0}} \cdot P_{D^0} \quad (24)$$

Thus, from Eqs.(24) and (6) one get for (23)

$$p_{\pi_s} < p_0 + \frac{(m_\pi + P^*)}{M_{D^0}} \cdot P_{D^0} \quad (25)$$

Instead of (25) it is possible to apply another, less strict cut

$$p_{\pi_s} < p_\pi^+(P_{max}) \simeq \frac{(m_\pi + P^*)}{M_{D^*}} \cdot P_{max} \quad (26)$$

here P_{max} is the right-hand edge of the kinematic range of the D^* candidates, $P_{D^*} < P_{max}$.

4 Pentaquark states

Now we apply the results of the previous sections to new resonances predicted [4] by Diakonov, Petrov and Polyakov in the framework of the chiral soliton model and detected both in the formation type [5] and in the production type [6] experiments.

4.1 $\Theta(1530) \rightarrow N(939) + K(498)$

With the mass value predicted for Θ^+ , $M_\Theta=1.530$ GeV, and the masses³ of decay products, $m_N=0.939$ GeV and $m_K=0.498$ GeV, the condition (9) is not satisfied. That implies the overlap of the m -bands at all P_Θ (Fig. 3a), as well as the overlap of the E -bands at $P_\Theta > \hat{P}_\Theta=2.15$ GeV (Fig. 3b). The overlapping is not strong and both selectors (11) and (19) work with high efficiency (see Fig. 4). The m - and E -selectors were already successfully applied in searches for the Θ^+ in production-type [6] and formation-type [7] experiments.

³In calculations were used mass values averaged over the isomultiplet.

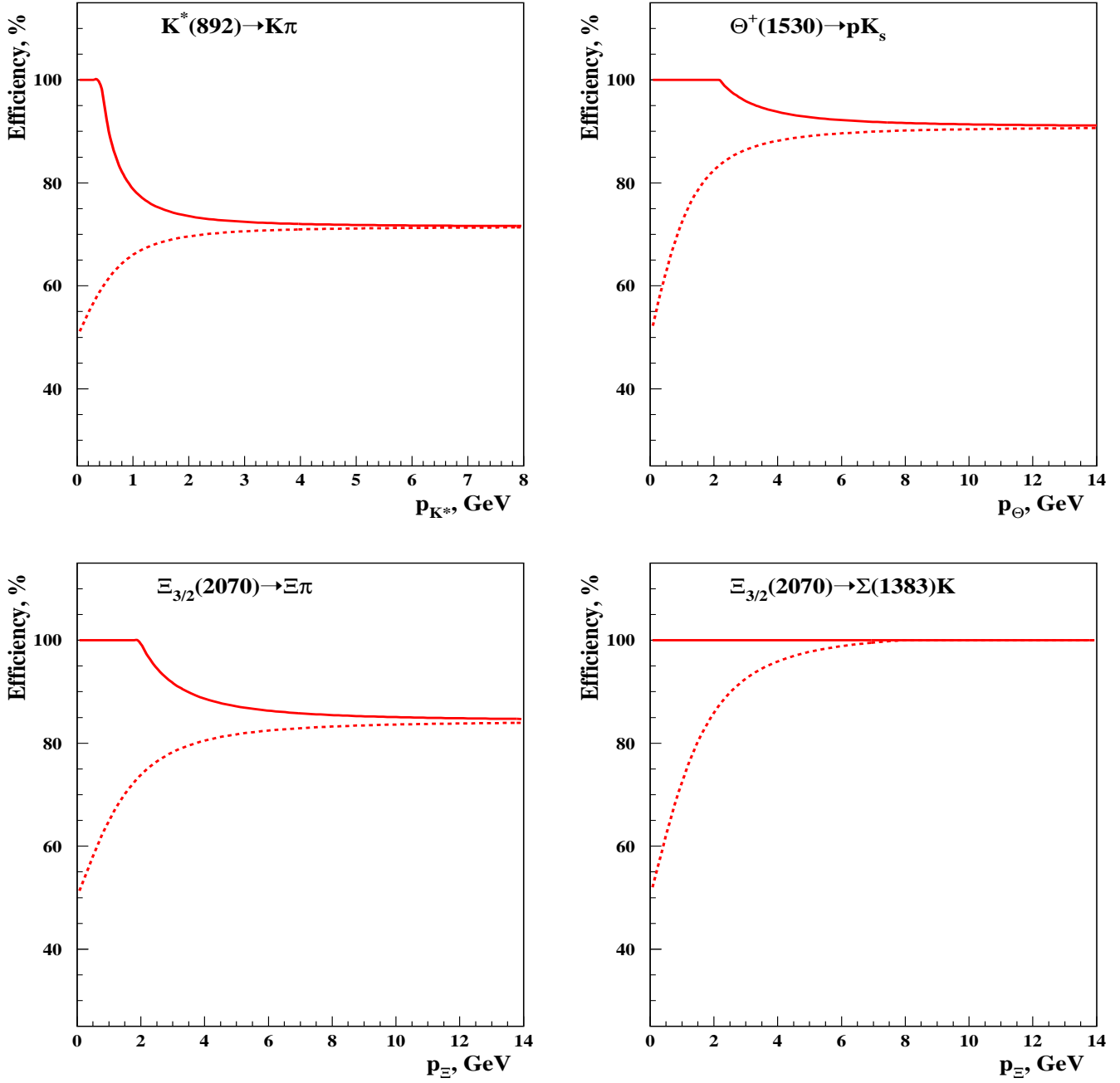


Figure 4: Efficiency of the selection rule $p_a > p_b$ (dashed line) and $E_a > E_b$ (full line) at different P_R in decays of $K^*(892)$, $\Theta(1530)$ and $\Xi_{3/2}(2070)$ resonances.

4.2 $\Xi_{3/2}(2070) \rightarrow \Xi(1318) + \pi(139)$

A baryonic state Ξ is a weakly decaying particle. In a cascade decay, the vertex of the decay $\Xi \rightarrow \Lambda\pi$ is separated from the primary vertex, similarly to $\Lambda \rightarrow p\pi^-$ decays. This property is

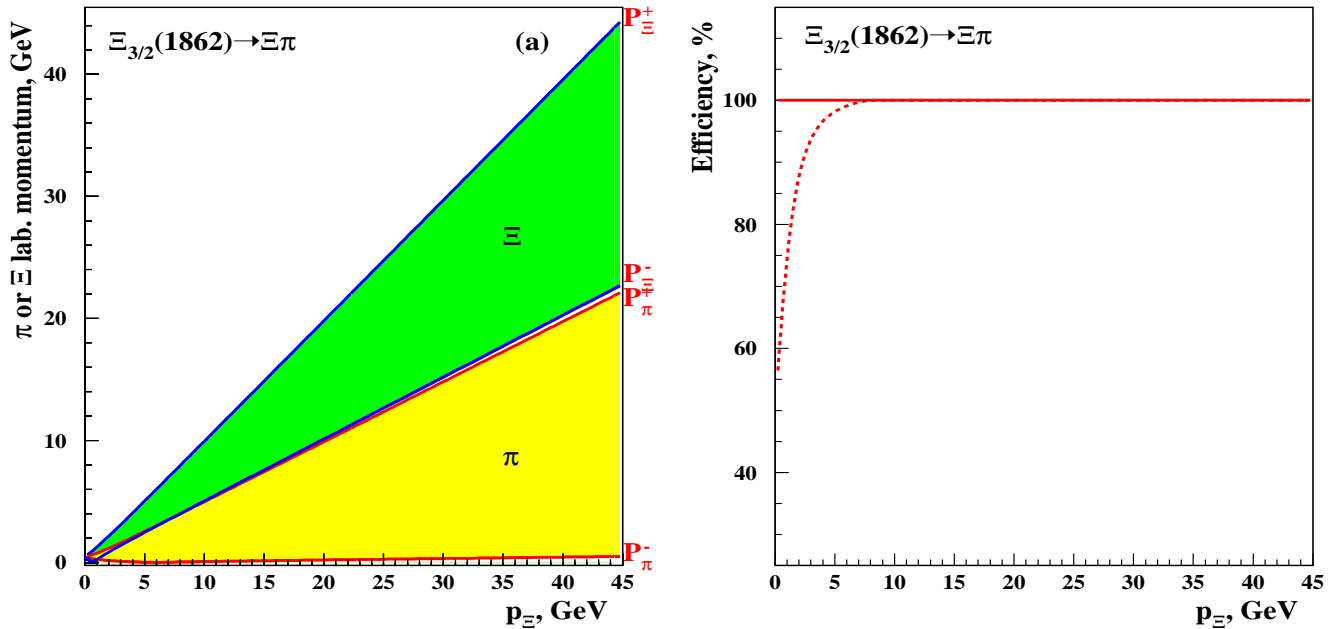


Figure 5: The m -bands and the efficiency of the m - and E -selectors for the $\Xi_{3/2} \rightarrow \Xi + \pi$ decay with the $\Xi_{3/2}$ mass reported by the NA49 collaboration [8].

used to suppress combinations which do not result from a Ξ decay and helps to reconstruct the Ξ candidate and its invariant mass.

In spite of the large mass asymmetry, $m_{\Xi} \gg m_{\pi}$, the conditions (9)-(10) are not fulfilled in $\Xi_{3/2}$ decays and the pictures of the m - and E -bands shown in Figs 3c, and 3d are very similar to those in Θ^+ decays. At low momenta the efficiency of the E -selector is 100%. The E -bands start overlapping at $P_{\Xi} > 1.96$ GeV. Thus, the efficiency of the E -selector is no worse than 84% (Fig.4).

4.3 $\Xi_{3/2}(2070) \rightarrow \Sigma(1385) + K(498)$

The $\Sigma(1385)$ decays strongly and exclusively at the primary event vertex. The decay modes $\Sigma^{\pm 0} \rightarrow \Lambda \pi^{\pm 0}$ are dominant. Therefore, after the reconstruction of Λ , the use of the m - or E -selector allows reconstruction of the $\Sigma(1385)$ with 100% efficiency (see Fig 1b, Fig. 2b).

Figs 3e and 3f shows the m - and E -bands in $\Xi_{3/2}(2070)$ decays. The m -bands slightly overlap at low P_{Ξ} and diverge at $P_{\Xi} > 7$ GeV. The E -bands are totally separated. Thus, in that decay mode, the m - and E -selectors work with 100% efficiency (see Fig. 4).

4.4 $\Xi_{3/2}(2070)$ or $\Xi_{3/2}(1860)$?

The NA49 collaboration is provided [8] the evidence for the existence of a narrow $\Xi^- \pi^-$ baryon resonance with mass of 1.862 ± 0.002 GeV. This state is considered as a candidate for the exotic pentaquark state $\Xi_{3/2}$. The reported mass value is much lower as predicted in [4]. The last developments in the theory of pentaquark states did not exclude the lower mass for the $\Xi_{3/2}$ [9]. There are also arguments [10] that the result of the NA49 collaboration perhaps is inconsistent with data collected over the past decades.

In Fig. 5 shown the m -bands and the efficiency. They are much the similar to those in Fig. 3e and Fig. 4d. The picture of the E -bands is also similar to Fig. 3f. Thus, the E -selector will not suppress the signal but suppress background at higher masses.

5 Conclusions

Kinematics of the two-body decay, $R \rightarrow \mathbf{a} + \mathbf{b}$, has been analyzed in terms of the phase space m - and E -bands. On the basis of many examples, in particular, the exotic anti-decuplet baryons (pentaquark states), it has been demonstrated that for $m_{\mathbf{a}} > m_{\mathbf{b}}$ the selection rules $p_{\mathbf{a}} > p_{\mathbf{b}}$ and $E_{\mathbf{a}} > E_{\mathbf{b}}$ can be with a high efficiency applied to reconstruct many resonances and to suppress backgrounds.

Acknowledgments

The author is indebted to P. Bussey and A. Geise for a reading of the manuscript and comments, and grateful to other colleagues from the ZEUS collaboration for useful discussions. Special thanks are due to P. Ermolov and A. Kubarovsky for discussions of preliminary results of the SVD collaboration. This study is partially supported by the RFBR under Grant no. 02-02-81023.

References

- [1] ZEUS Collaboration; S. Chekanov et al., Phys. Lett. **B 578**, 33 (2004); Preprint DESY-03-098
- [2] G.I Kopilov, *Basics of resonance kinematics* (in Russian), Nauka, 1970; E.Byckling and K.Kajantie, *Particle kinematics*, John Wiley&Sons, 1972
- [3] Particle Data Groupe, K. Hagiwara et al., *Review of particle physics*. Phys. Rev. **D 66**, 010001 (2002)
- [4] D.Diakonov, V.Petrov and M.V. Polyakov, Z.Phys. **A 359**, 305 (1997).
- [5] LEPS Collaboration, T. Nakano et al., Phys. Rev. Lett. **91**, 012002 (2003); CLAS Collaboration, S. Stepanyan et al., arXiv:hep-ex/0307018; CLAS Collaboration, V. Kubarovsky *et al.*, arXiv:hep-ex/0311046; SAPHIR Collaboration, J. Barth et al., Phys. Lett. **B 572**, 127 (2003); A. E. Asratayn, A. G. Dolgolenko and M. A. Kubantsev, arXiv:hep-ex/0309042; DIANA Collaboration, V.V. Barmin et al., Phys. Atom. Nucl. **66**, 1715 (2003); HERMES Collaboration, A. Airapetian et al., arXiv:hep-ex/0312044 and DESY-03-213
- [6] ZEUS Collaboration., S. Chekanov, a talk at "DESY Forum: Pentaquarks at HERA", DESY, Hamburg, November, 25, 2003. <http://webcast.desy.de>
- [7] SVD Collaboration., P.Ermolov, private communication.
- [8] NA49 Collaboration, C. Alt et al., arXiv:hep-ex/0310014
- [9] M. Polyakov, a talk at "DESY Forum: Pentaquarks at HERA", DESY, Hamburg, November, 25, 2003. <http://webcast.desy.de>
- [10] H.G. Fischer and S. Wenig, arXiv:hep-ex/0401014